
PLUMAGE:

Probabilistic Low-rank Unbiased Min-Variance Gradient Estimator for Efficient Large Model Training

Matan Haroush

Department of Electrical Engineering
Technion
Haifa, Israel
matan.h@campus.technion.ac.il

Daniel Soudry

Department of Electrical Engineering
Technion
Haifa, Israel
daniel.soudry@gmail.com

Abstract

Accelerator memory and networking constraints have emerged as dominant bottlenecks when training *large language models* (LLMs) with billions of parameters. Existing low-rank gradient estimators such as GALORE and FLORA compress gradients and optimizer tensors by projecting weight-gradients onto a rank- r subspace, enabling LLM training on consumer hardware. Yet, these methods are either biased or subject to high estimator variance. Moreover, the optimizer state based on the first *and* second-moment estimates expressed in the previous subspace becomes misaligned whenever the projection is updated, leading to instabilities during training. We propose **PLUMAGE: Probabilistic Low-rank Unbiased Minimum-variance Gradient Estimator**. PLUMAGE is a drop-in replacement for existing low-rank gradient estimators; it does not introduce new hyperparameters beyond the chosen rank r and the update interval τ . In addition, we resolve optimizer state misalignment issues to prevent spurious weight updates and enhance training stability. We empirically demonstrate that PLUMAGE shrinks the full-rank optimization’s gap over the pre-training evaluation loss by 33% on average across models, and the average training loss across the GLUE benchmark by 28% – within a similar computational and memory footprint as GaloRE.

1 Introduction

Natural language modeling has benefited from training large-language models (LLMs), which consist of billions of parameters on massive amounts of unsupervised data. This typically requires distributed training algorithms employing tens of thousands of interconnected high-end accelerators to speed up the training time. Moreover, some of the largest state-of-the-art models do not fit in a single device’s memory. Meanwhile, the historical progress of scaling the capabilities of high-bandwidth memory and device connectivity lags behind progress in scaling the compute capabilities of modern accelerators [14]. Thus, significant engineering and research efforts aim to improve the efficiency of training and inference. For example, a variety of methods have been proposed, leveraging model parallel computing [31, 26, 40], structured sparsity [18, 7], and applications of low-precision numerical formats [8, 3, 6, 9, 4].

As models grow in size, the memory and connectivity limitations of modern accelerators emerge as a critical bottleneck, impeding the ability of the research community to train and fine-tune state-of-the-art models without relying on access to expensive hardware and infrastructure. Addressing these constraints is essential for reducing entry barriers for future research. One recent avenue of work aims to enable the training and fine-tuning of large models with limited accelerator memory overhead. For example, parameter-efficient fine-tuning methods inject trainable adapters into frozen

large models when learning a new task. For instance, Hu et al. [17] (LoRA) proposed attaching low-rank parametrized adapters to the linear layers of a given model to augment its activations. This approach reduces optimizer state memory requirements compared to full model training, reduces the risk of overfitting on small datasets, and potentially incorporates compute and memory gains from low-bit numerical formats (e.g., QLoRA, Dettmers et al. [10]). However, these methods rely on having a pre-trained model and are less suited when one wishes to train the entire model.

Recently, Zhao et al. [39] (GALORE) proposed projecting gradients to a low-rank subspace. The method projects the dense linear layers’ weight gradients, reducing the optimizer’s state memory without enforcing a low-rank weight structure, leading to a potentially better compression rate and lower terminal loss. More importantly, the authors showed how large language models can be trained from scratch on widely available consumer-grade hardware with limited memory. Notably, the gradient projection at the core of the method is constructed by stacking the top- k singular vectors of the weight gradient that are periodically computed via Singular Value Decomposition (SVD, Eckart and Young [11]).

These results led us to question whether there is a better low-rank gradient estimation alternative for training neural networks, given that the gradients are not necessarily of low rank. Moreover, fixing the projection to the span of the top- k singular vectors can lead to a significant accumulation of bias during the optimization process, which is known to be detrimental [6, 5]. Our contributions can be summarized as follows:

- We derive a novel k -sparse **Probabilistic Low-rank Unbiased Minimum-vAriance Gradient Estimator** (PLUMAGE). Our approach relies on an efficient and fixed-rank sampling strategy without replacement. In addition, it requires permanent storage of only a one-sided projection matrix per weight, similarly to Zhao et al. [39].
- We develop an alignment method for the first and second moments used by stateful optimizers such as ADAM. Our alignment strategy mitigates the adverse effects of periodic projection subspace updates during training and enhances the training stability with low-rank gradient estimators.
- We empirically demonstrate a significant improvement in convergence when using low-rank gradient estimators — without tuning the full-rank learning rate or adding hyperparameters other than the rank of choice and projection update interval.

2 Related Work

This section contains foundational and closely related work necessary to contextualize our approach.

Momentum and Adaptive Optimizers. Given learning rate η and the gradient $\mathbf{G}_t = \nabla \mathcal{L}_t$ at step t , vanilla stochastic gradient descent (SGD) updates the weight matrix in each layer according to

$$\mathbf{W}_{t+1} = \mathbf{W}_t - \eta \mathbf{G}_t. \quad (1)$$

Adding a momentum term with a β_1 coefficient to dampen stochastic gradient noise (SGDM, Rumelhart et al. [27]) yields

$$\mathbf{M}_t = \beta_1 \mathbf{M}_{t-1} + (1 - \beta_1) \mathbf{G}_t \quad (2)$$

$$\mathbf{W}_{t+1} = \mathbf{W}_t - \eta \mathbf{M}_t. \quad (3)$$

In adaptive step-size optimizers, the learning rate is adjusted based on past gradients. For instance, ADAM [20] update rule is

$$\mathbf{V}_t = \beta_2 \mathbf{V}_{t-1} + (1 - \beta_2) \mathbf{G}_t^{\circ 2} \quad (4)$$

$$\mathbf{W}_{t+1} = \mathbf{W}_t - \frac{\eta \mathbf{M}_t}{\sqrt{\mathbf{V}_t} + \epsilon}. \quad (5)$$

where \mathbf{V}_t is the second-moment estimate of the gradients, and $\square^{\circ 2}$ denotes element-wise square (bias-correction factors omitted).

Memory-Efficient Optimizers. Despite its popularity and advantages, ADAM incurs a high computational and memory overhead. Light-state optimizers such as Adafactor [30] and subsequent (e.g., Lion, Shampoo, etc., [5, 15, 34]), were introduced to mitigate this overhead. An alternative approach is to quantize the state optimizers (e.g., Dettmers et al. [9]). These methods are generally orthogonal to our work since they can be applied to a low-rank gradient as input.

Sparse Gradients. Sparse gradient methods such as coordinate descent focus on updating only a subset of model parameters, reducing compute, communication, and memory costs by dropping parts of the gradient (e.g., [1, 7]). Recently, Muhamed et al. [24] proposed an efficient and light sparse gradient method dubbed GRASS. GRASS maintains row-sparse gradient statistics in its optimizer state. It is constructed as an unbiased and minimum variance gradient estimator by selecting rows according to their norm. However, the minimum variance property is under a multinomial sampling. The authors point out that analytically computing the minimum variance for a multinomial distribution without replacement is not tractable. Ultimately, allowing high norm rows to be sampled multiple times increases the estimator variance compared to non-replacement sampling. In addition, a row-sparse approach leads to instabilities during training. As a result, the authors resort to strategies such as momentum restarts and periodic learning-rate warm-ups when updating the sampled row indices.

Low-Rank Gradients for Communication Compression. In distributed settings, low-rank gradient methods project the gradients onto a lower-dimensional subspace when synchronizing the gradients between the workers before performing an optimization step. For example, Wang et al. [36] (ATOMO) proposed a min-variance unbiased low-rank gradient estimator that reduces communication by sparsifying the gradient’s singular values and transmitting only the surviving SVD components. ATOMO’s sampling strategy produces a rank- k gradient *on average* and requires communication of both the left and right projections. Later, PowerSGD [33] leveraged the power-iteration method to maintain an approximation of the top- k gradient singular vectors, reducing the cost of applying SVD on the gradients before each communication, while adding a feedback mechanism to incorporate the previous step error in the next gradient communication.

Low-Rank Gradients for Memory-Constrained Optimization. GALORE and FLORA exploit the low-rank gradient structure to reduce device memory costs [39, 16] when training and finetuning large models that do not fit in the device memory. Unlike previously mentioned GALORE, FLORA utilizes reconstructible random Gaussian projections (via random generator seed reuse) and is paired with ADAFACTOR [30] optimizer, which maintains a factorized approximation of the second moment statistic used for the adaptive step-size. As such, it only maintains the projected gradient moment in memory. FLORA’s low-rank gradient moment estimation is unbiased, assuming projections are updated frequently enough; however, the application of random projection matrices yields an additive variance proportional to the number of trainable parameters. Thus, it is less suited for training large models from scratch. The authors address this caveat by setting a low update frequency, trading off bias for variance while focusing on small model training and fine-tuning tasks. Recently, Shamshoum et al. [28] (DROPACT) proposed applying a random projection (similarly to FLORA) to the linear layer’s inputs during the forward phase before storing them for the backward phase to further reduce input memory for the weight gradient. This approach reduces activation, gradients, and optimizer state memory as the gradients are only projected back for weight update. We will later show (Section 4.3) that FLORA typically leads to a higher loss than both GALORE and our method. We attribute this primarily to the high variance incurred by sampling high-dimensional random projections.

In continuation to GALORE, Liao et al. [22] (GALORE+) proposed reducing the SVD overhead by leveraging randomized SVD approximation for the top- k singular vectors, along with sparse coding of the low-rank residual errors and sharing of projection matrices across attention heads weights in the same layer. The proposed method is focused on accelerating fine-tuning of LLMs, and its results are on par with GALORE. Finally, Liang et al. [21] suggested improving low-rank gradient estimators’ performance by tracking the gradient subspace by an online PCA approach. This approach is designed to reduce the cost of frequent SVD, however, the online PCA cost is added to each iteration. Both methods are ultimately biased due to the accumulation of approximation error of the top- k singular vectors.

3 PLUMAGE: Min-Variance, Unbiased, and Low-Rank Estimator

The following section is dedicated to developing the min-variance unbiased low-rank gradient estimator, following similar design considerations as in [2, 36, 7] while emphasizing favorable characteristics for optimization with low-rank gradients. Namely, a fixed target rank leading to a deterministic compute cost, and to use only a one-sided projection matrix to minimize required storage. Finally, we establish PLUMAGE’s efficient sampling strategy and develop the tools for deploying PLUMAGE in stateful optimizers such as ADAM.

3.1 MVUE: Min-Variance, Unbiased and Low-Rank Estimator

Given the matrix $\mathbf{G} \in \mathbb{R}^{m \times n}$ and its singular values decomposition $\mathbf{G} = \sum_{i=1}^n \sigma_i \mathbf{u}_i \mathbf{v}_i^\top$, where $n \leq m$ and $\sigma = \{\sigma_i\}_{i=1}^n$ is ordered from largest to smallest singular values. The classic low-rank estimator based on the top- k singular vectors with $k \leq n$ is given by

$$\hat{\mathbf{G}}_{\text{top-}k} = \sum_{i=1}^k \sigma_i \mathbf{u}_i \mathbf{v}_i^\top \quad (6)$$

is known to have the minimal mean square error [11]. However, the error due to the truncation of the tail components results in a bias. It was also known that gradient bias is detrimental to the optimization process, as errors are accumulated over multiple training iterations [6, 7]. Therefore, we consider a low-rank gradient estimator with the general form

$$\hat{\mathbf{G}} = \sum_{i=1}^n \frac{1}{p_i} I_i \sigma_i \mathbf{u}_i \mathbf{v}_i^\top \quad (7)$$

where I_i are indicator function for including the i^{th} singular vector while p_i are scalar constants. We aim to find a distribution for I_i such that the following properties hold:

1) Unbiased gradient estimator:

$$\mathbb{E} \hat{\mathbf{G}} = \mathbf{G} \Leftrightarrow p_i = \mathbb{E} I_i \quad (8)$$

2) Deterministically of k -rank:

$$\sum_{i=1}^n I_i = k \Rightarrow \sum_{i=1}^n p_i = k \quad (9)$$

3) Minimal variance:

$$\min_{\hat{\mathbf{G}}} \mathbb{E} \text{Tr} \left[\left(\hat{\mathbf{G}} - \mathbb{E} \hat{\mathbf{G}} \right)^\top \left(\hat{\mathbf{G}} - \mathbb{E} \hat{\mathbf{G}} \right) \right] \quad (10)$$

To minimize the expected variance, we plug the estimator definition from Eq. (7) into Eq. (10) and, using the orthogonality of the singular vectors, we obtain $\mathbf{v}_i^\top \mathbf{u}_j = \delta_{ij}$,

$$\mathbb{E} \text{Tr} \left[\sum_{i,j=1}^n \left(\frac{I_i}{p_i} - 1 \right) \left(\frac{I_j}{p_j} - 1 \right) \mathbf{u}_i \mathbf{v}_i^\top \mathbf{u}_j \mathbf{v}_j^\top \sigma_i \sigma_j \right] = \mathbb{E} \text{Tr} \left[\left(\sum_{i=1}^n \left(\frac{I_i}{p_i} - 1 \right)^2 \sigma_i^2 \mathbf{u}_i \mathbf{v}_i^\top \right) \right] \quad (11)$$

$$= \mathbb{E} \left(\sum_{i=1}^n \left(\frac{I_i}{p_i} - 1 \right)^2 \sigma_i^2 \mathbf{v}_i^\top \mathbf{u}_i \right) = \sum_{i=1}^d \left[\mathbb{E} \left(\frac{I_i}{p_i} - 1 \right)^2 \right] \sigma_i^2 = \sum_{i=1}^d \left[\left(\frac{1}{p_i} - 1 \right) \right] \sigma_i^2 \quad (12)$$

Taking into account the sparsity condition in Eq. (9), we define \mathbf{p} as the indicator probabilities vector that minimizes the variance in Eq. (12). We find \mathbf{p} by solving the following problem

$$\min_{\mathbf{p}} \sum_{i=1}^n \left[\left(\frac{1}{p_i} - 1 \right) \right] \sigma_i^2 \text{ s.t. } \sum_{i=1}^n p_i = k, p_i \in [0, 1] \quad (13)$$

which is equivalent to

$$\min_{\mathbf{p}} \sum_{i=1}^n \frac{\sigma_i^2}{p_i} \text{ s.t. } \sum_{i=1}^n p_i = k, p_i \leq 1 \quad (14)$$

Note that we cannot allow for $p_i = 0$ since then the optimization objective is undefined. To solve Eq. (14), we write the Lagrangian

$$\sum_{i=1}^n \frac{\sigma_i^2}{p_i} + \mu \sum_{i=1}^n p_i + \sum_{i=1}^n \lambda_i p_i \quad (15)$$

where $\mu > 0, \lambda_i > 0$ are the Lagrangian factors, and after differentiating by p_i we get

$$0 = -\frac{\sigma_i^2}{p_i^2} + \mu + \lambda_i \Rightarrow p_i = \frac{\sigma_i}{\sqrt{\mu + \lambda_i}} \quad (16)$$

Note that $\lambda_i > 0$ only if we hit the inequality constraints, i.e., $p_i = 1$. To satisfy the constraints, we first solve

$$r^*(k, \sigma) = \arg \min_{r \in \{0, \dots, d\}} r \text{ s.t. } \frac{(k-r)\sigma_{r+1}}{\sum_{i=r+1}^n \sigma_i} < 1 \quad (17)$$

Then, we return the following solution

$$p_i = \begin{cases} 1 & , \text{ if } i \leq r^* \\ \frac{(k-r^*)\sigma_i}{\sum_{j=r^*+1}^n \sigma_j} & , \text{ if } i > r^* \end{cases} \quad (18)$$

It is important to note that I_i need not be independent. Meaning, that we can sample the singular vectors however we want, just as long as we satisfy Eq. (18) (e.g. to satisfy the k -sparse condition in Eq. (9)). For example, we can first sample $i = 1 \dots r^*$ (deterministically), then sample a $(k - r^*)$ sparse solution from the rest of the components. Specifically, let $k \leq n$ and $\{p_i\}_{i=1}^n$ a series of the singular vectors inclusion probabilities, with $p_i \in (0, 1)$ and $\sum_{i=1}^n p_i = k$. We wish to sample without replacement exactly k distinct indices $I \triangleq \{i_1 \dots i_k\}$ such that $\forall i \in \{1 \dots n\} : \mathbb{P}(i \in I) = p_i$. To this end, we employ a “wheel-of-fortune” sampling trick with k equidistant arms [12] to efficiently sample projections. Namely, we shuffle the order of p_i , then each p_i is represented by an angular sector that is proportional to $\frac{p_i}{\sum_{k=1}^n p_k}$. Finally, the arms are randomly rotated (with uniformly distributed shift) to extract all the indices in a single step. The sampling algorithm is illustrated in Fig. 1. Computing \mathbf{p} and sampling can be implemented efficiently in $\mathcal{O}(\min(m, n))$ and is negligible compared to SVD computation.

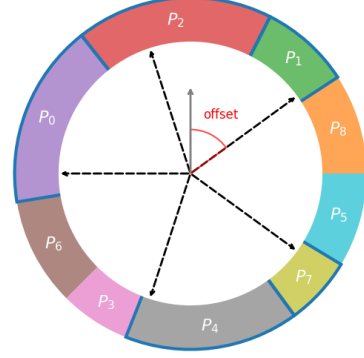


Figure 1: “Wheel-of-Fortune” sampling with $k = 5$ arms

3.2 One-sided PLUMAGE

Next, we move to construct an estimator using only a one-sided projection and show that our one-sided estimator maintains the MVUE properties. Without loss of generality, we assume our gradient estimator is based on a left-sided projection \mathbf{P} . The projection matrix is constructed by stacking the sampled singular values,

$$\mathbf{P} = \begin{bmatrix} \underbrace{\mathbf{u}_1 I_1}_{\text{column 1}} & \dots & \underbrace{\mathbf{u}_d I_d}_{\text{column } d} \end{bmatrix}. \quad (19)$$

Similarly, right-sided projections stack \mathbf{v}_i singular vectors as rows. Next, given the diagonal scaling matrix $\mathbf{D} = \text{Diag}(p_1, p_2, \dots, p_d)$, the one-sided estimator for a matrix \mathbf{G} is given by

$$\hat{\mathbf{G}} = \mathbf{P} \mathbf{D}^{-1} \mathbf{P}^\top \mathbf{G} = \sum_{i=1}^n \frac{1}{p_i} I_i \mathbf{u}_i \mathbf{u}_i^\top \mathbf{G}. \quad (20)$$

Finally, we plug in $\mathbf{G} = \sum_{i=1}^n \sigma_i \mathbf{u}_i \mathbf{v}_i^\top$. Through the orthonormality of the singular vectors, we recover

$$\hat{\mathbf{G}} = \sum_{j=1}^n \sigma_j \sum_{i=1}^n \frac{1}{p_i} I_i \mathbf{u}_i \mathbf{u}_i^\top \mathbf{u}_j \mathbf{v}_j^\top = \sum_{j=1}^n \sigma_j \sum_{i=1}^n \delta_{ij} \frac{1}{p_i} I_i \mathbf{u}_i \mathbf{v}_j^\top = \sum_{i=1}^n \frac{1}{p_i} I_i \sigma_i \mathbf{u}_i \mathbf{v}_i^\top. \quad (21)$$

Since Eq. (21) is equivalent to the original formulation from Eq. (7), the one-sided projection has the same properties as the two-sided variant.

3.3 Incorporating PLUMAGE in Optimizers

We apply PLUMAGE to compress the optimizer’s first and second momentum, which are common statistics tracked by optimizers such as ADAM and SGDM.

3.3.1 Low-rank moments and ADAM weight update

The low-rank moments are given by

$$\mathbf{M}_t^l = \beta_1 \mathbf{M}_{t-1}^l + (1 - \beta_1) \mathbf{P}_t^\top \mathbf{G}_t \quad (22)$$

$$\mathbf{V}_t^l = \beta_2 \mathbf{V}_{t-1}^l + (1 - \beta_2) (\mathbf{P}_t^\top \mathbf{G}_t)^{\circ 2}, \quad (23)$$

and the simplified low-rank ADAM update rule is

$$\mathbf{W}_{t+1} = \mathbf{W}_t - \eta \mathbf{P}_t \mathbf{D}_t^{-1} \frac{\mathbf{M}_t^l}{\sqrt{\mathbf{V}_t^l + \epsilon}}, \quad (24)$$

where $\mathbf{P}_t \in \mathbb{R}^{m \times r}$ denotes the left projection matrix composed from the singular vectors of \mathbf{G}_t and \mathbf{D}_t is similarly the diagonal matrix containing its sampled singular values, as explained in Section 3.2.

3.3.2 Design considurations

We wish to amortize costly SVD by reusing the same projection over multiple optimizer steps, similarly to Zhao et al. [39]. Given the hyperparameter $\tau \in \mathbb{N}^+$, the interval length between subsequent SVD. For notation convenience, we define the index mapping $k_t = \lfloor t/\tau \rfloor$. We define the optimizer statistics as

$$\mathbf{M}_t^{l k_t} = \beta_1 \mathbf{M}_t^{l k_t} + (1 - \beta_1) \mathbf{P}_{k_t} \mathbf{G}_t \quad (25)$$

$$\mathbf{V}_t^{l k_t} = \beta_2 \mathbf{V}_t^{l k_t} + (1 - \beta_2) (\mathbf{P}_{k_t} \mathbf{G}_t)^{\circ 2} \quad (26)$$

$$\mathbf{W}_{t+1} = \mathbf{W}_t - \eta \mathbf{P}_{k_t} \mathbf{D}_{k_t}^{-1} \frac{\mathbf{M}_t^{l k_t}}{\sqrt{\mathbf{V}_t^{l k_t} + \epsilon}}. \quad (27)$$

The projection \mathbf{P}_{k_t} and scaling factors \mathbf{D}_{k_t} are sampled once after computing SVD over \mathbf{G}_{k_t} according to the probability p_{k_t} computed according to Eq. (18). In this case, p_{k_t} is no longer proportional to \mathbf{G}_{k_t} 's singular values. Thus, we lose the minimum variance promise of PLUMAGE; however, the estimate remains unbiased so long as $\#total_training_steps \gg \tau$ (i.e., the projections are resampled often enough, albeit additional SVD is not required as we explain next). Moreover, note that PLUMAGE needs only to store the diagonal elements in \mathbf{D}_{k_t} up to the chosen rank, contributing to minor memory overhead compared to the baseline GALORE memory cost.

If the gradient subspace changes slowly during optimization, we can still benefit from variance reduction. In addition, one can also define the $\kappa \in \mathbb{N}^+$ hyperparameter to introduce a resampling interval that refreshes the projection and scaling coefficients without computing the SVD (i.e., $\kappa \leq \tau$). This can help balance subspace exploration and SVD compute overhead under the uncertainty of how well the sampled subspace retains the information from the observed gradients. In our experiments, sampling projection once throughout the SVD update interval works well. Yet, we found that overly frequent projection updates may hurt the utility of the moment statistics in the optimization process. We leave the exploration of this tradeoff for future work and set $\kappa = \tau$ in our experiments. In addition, we explored methods for measuring the subspace correlation with the recent gradients in the appendix.

3.3.3 Statistics realignment of the first and second moments

Stateful optimizers such as ADAM, when using low-rank estimators such as GALORE, suffer from a crucial subspace alignment issue when the gradient's projection is updated during training. In essence, the low-rank statistics represent moment estimates tracked in different subspaces. Formally, let $\mathbf{G}^t = \mathbf{P}_t^\top \mathbf{G}$ then, $\mathbf{M}^t = \mathbb{E} [\mathbf{G}^t]$ and $\mathbf{V}^t = \mathbb{E} [(\mathbf{G}^t)^{\circ 2}]$. However, given two arbitrary projection metrics $\mathbf{P}_1 \in \mathbb{R}^{m \times r_1}$ and $\mathbf{P}_2 \in \mathbb{R}^{m \times r_2}$, it is clear that $\mathbf{M}^1 \neq \mathbf{M}^2$ and $\mathbf{V}^1 \neq \mathbf{V}^2$. For instance, if $\mathbf{P}_1 \perp \mathbf{P}_2$, then \mathbf{M}^1 has no information on \mathbf{M}^2 . Moreover, misalignment can occur even if the subsequent projections span the same subspace (e.g., a rotation of the singular vectors). Therefore, updating the projections without statistics realignment may lead to spurious weight updates in the following weight updates (until the new data is sufficiently represented in the first and second moment estimators). Similarly to Hao et al. [16], one can initialize \mathbf{M}^2 , after

updating the projection, by projecting the previous estimate onto the shared subspace between the two projections to realign the first-moment statistics,

$$\mathbf{M}^{l2} \approx \mathbf{P}_2^\top \mathbf{P}_1 \mathbf{M}^{l1} \quad (28)$$

Notably, unlike Hao et al. [16], under PLUMAGE’s \mathbf{P}_i are orthonormal matrices. Thus, $\mathbf{B} = \mathbf{P}_2^\top \mathbf{P}_1$ projects \mathbf{M}^{l1} onto the intersection of subspaces induced by the projections \mathbf{P}_i . The resulting \mathbf{M}^{l2} magnitude will be proportional to the cosine of the principal angle between the two subspaces since $\|\mathbf{B}\| \leq 1$. Moreover, when \mathbf{P}_i spans the same subspace, the transformation rotates the moment without distortion since $\|\mathbf{B}\| = 1$. For \mathbf{V}^{l2} , one cannot simply initialize $\mathbf{V}^{l2} = \mathbf{B}\mathbf{V}^{l1}$ after the change in projections, since it will produce negative entries. Since finding the optimal inverse projection is not trivial, we devise an approximation for \mathbf{V}^{l2} as an initial guess.

$$\mathbf{V}_{ij}^{l2} = \mathbb{E} \left[\mathbf{B} \mathbf{G}^{l1} \right]_{ij}^2 = \sum_{k,l} B_{ik} B_{il} \mathbb{E} \left[G_{kj}^{l1} G_{lj}^{l1} \right] \approx \sum_{l,k} B_{ik} B_{il} \mathbb{E} \left[\left(G_{kj}^{l1} \right)^2 \right] = \left[\mathbf{B}^{\circ 2} \mathbf{V}^{l1} \right]_{ij}, \quad (29)$$

where in the \approx step we approximated the gradient’s second-moment matrix to be diagonal, i.e., $\mathbb{E} [G_{kj} G_{lj}] \approx 0$ for $k \neq l$. Such a diagonal approximation is commonly used in both theory and practice [20, 19]. In Section 4.1, we empirically demonstrate that our initialization produces better results than simply assuming $\mathbf{M}^{l1} \approx \mathbf{M}^{l2}$ and $\mathbf{V}^{l1} \approx \mathbf{V}^{l2}$ when updating the gradient projection.

A full algorithm demonstrating how to incorporate PLUMAGE in ADAM optimizer is given in Algorithm 5 in the appendix.

4 Experiments

4.1 PLUMAGE Ablation Study

Similarly to Zhao et al. [39], we evaluate the optimization performance of our Adam-based PLUMAGE optimizer by pre-training LLaMA with varying sizes on the C4 English dataset from scratch. In all C4 English experiments, we rely on the processed version of the ‘‘Colossal Cleaned Crawl’’, which is readily available in the Huggingface datasets library [37, 13, 25]. As in Zhao et al. [39], we split the full-length training and validation examples into segments with 256 tokens per example using the T5 tokenizer from Raffel et al. [25].

Specifically, we set the learning rate to 10^{-3} and $\beta_1, \beta_2 \leftarrow 0.9, 0.999$, while the low-rank gradient estimators’ additional hyperparameters are set to $r, \tau, \alpha \leftarrow 128, 200, 1.0$, where τ is the interval between projection updates, and α is the learning rate scale applied only to the low-rank layer weights in GALORE

The ablation results (Table 1, Fig. 2a) include the base PLUMAGE (Eq. (27)), the ‘first Momentum Projection realignment’ method (Eq. (28)) tagged with MP, and the ‘Second moment realignment’ (Eq. (29)) method tagged with S/MP.

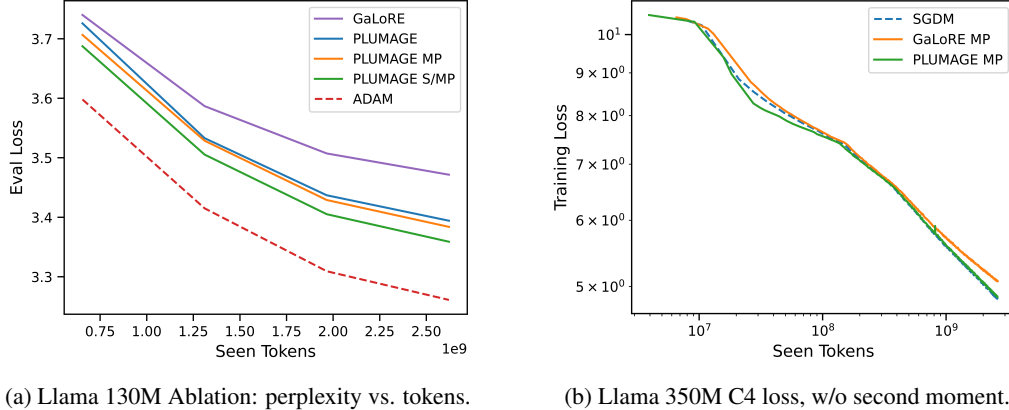
Table 1: Ablation: terminal loss and accuracy observed on Llama 130M after 2.6B Tokens.

	Train Loss	Eval Loss	Accuracy
ADAM	3.256	3.256	38.7
GALORE	3.473	3.471	36.5
PLUMAGE	3.402	3.400	37.1
PLUMAGE _{MP}	3.386	3.385	37.3
PLUMAGE _{S/MP}	3.378	3.377	37.4

An optimization gap between the low-rank gradient optimizers and the full-rank ADAM is apparent. However, PLUMAGE_{S/MP} shrinks the gap between the GALORE and Adam baseline by a factor of ~ 2 when not tuning the hyperparameters from the baseline training regime (that Zhao et al. [39] found to be optimal for ADAM).

4.2 PLUMAGE debias impact

While PLUMAGE is unbiased, applying it to ADAM does not produce unbiased gradients due to the use of the non-linear adaptive scaling factor based on the \mathbf{V} statistic. The \mathbf{V} term contributes to gradient bias with the ADAM update as well, thus degradation observed in Table 1 is expected. To better understand how bias impacts optimization with low-rank gradients, we train a medium-sized Llama variant with 350M parameters on 2.6B tokens from the C4 English dataset as before. However,



(a) Llama 130M Ablation: perplexity vs. tokens.

(b) Llama 350M C4 loss, w/o second moment.

Figure 2

since the adaptive step size is biased, we use stochastic gradient descent with momentum (SGDM). This is achieved by disabling the second-moment term in Adam and comparing it with the adapted versions of PLUMAGE_{MP} and GaLoRE_{MP} variants. We use momentum $\beta = 0.9$ for all optimizers and a learning rate of 0.1. In addition, we fix the projection intervals to 200 steps and the rank to 128, while the hidden dimension of the model is 1024. In Section 4.2, we observe the training loss on a log scale. Our version of SGDM + PLUMAGE_{MP} convergence rate is on par with the full-rank SGDM optimizer, while it is clear that SGDM + GaLoRE_{MP} bias is impeding the optimization.

4.3 Fine-tuning with Low-Rank Gradients

Following Zhao et al. [39] and Hao et al. [16], we evaluate the low-rank optimization on the standard GLUE natural understanding benchmark [35]. We fine-tune all parametrized layers in the Roberta base model [23] except for its embedding layers, while low-rank gradient estimators are used for all linear layers’ weights. We fix the rank $r = 8$, and reuse the hyperparameters as suggested in Zhao et al. [39]. In particular, the update interval $\tau = 100$ and the recommended α scales for GaLoRE (recall that PLUMAGE does not use α). We optimize the model for 30 epochs for each task with individually tuned learning rates for each method as done in Zhao et al. [39]. Finetuning longer than the usual number of epochs ensures the loss has converged. This allows us to compare the terminal loss between the different estimators to evaluate the estimators’ impact on the optimization gap. The results are reported in Table 2, where for each task we show the best metrics for accuracy and loss. Again, a training error gap exists in all low-rank fine-tuning methods since a bias exists in all adaptive optimizers. It is also notable that replacing GaLoRE with PLUMAGE leads to lower or equivalent terminal loss and next token prediction accuracy.

Table 2: Fine-tuning RoBERTa-Base on GLUE benchmark. We present the best terminal accuracy (and loss) metrics for each task after 30 epochs over 5 learning rates for each optimizer.

	MNLI	QQP	QNLI	SST-2	CoLA	STS-B	MRPC	RTE	Mean
ADAM	87.60 (0.004)	89.35 (0.002)	92.86 (0.002)	94.27 (0.004)	63.58 (0.004)	90.92 (0.03)	92.93 (0.001)	75.81 (0.003)	85.91 (0.004)
FLORA	87.07 (0.25)	87.77 (0.15)	92.33 (0.15)	94.84 (0.07)	59.31 (0.13)	89.95 (0.22)	91.42 (0.16)	71.84 (0.24)	84.32 (0.16)
GaLoRE	85.78 (0.29)	85.46 (0.21)	91.95 (0.11)	92.78 (0.08)	62.32 (0.07)	90.75 (0.09)	91.36 (0.02)	78.70 (0.04)	84.89 (0.11)
PLUMAGE _{S/MP}	87.58 (0.22)	88.23 (0.13)	92.62 (0.06)	94.72 (0.05)	61.57 (0.03)	90.94 (0.09)	91.29 (0.005)	78.34 (0.02)	85.66 (0.08)

4.4 Pre-training language models from scratch

The pre-training process of LLMs involves digesting trillions of tokens, setting a high bar for model quality. It is challenging to replicate such experiments, particularly on consumer-grade equipment. However, exploring the dynamics of training large models from scratch is crucial for facilitating research into more efficient methods for training at scale. Thus, we attempt to train the models to a point where we can gain insight into the performance of different low-rank gradient optimizers.

We follow Zhao et al. [39] and pre-train several Llama variants with 130M, 350M, and 1B parameters on the C4 English dataset [13, 25]. We reuse the training regime and the best hyperparameters reported in [39] for GALORE and ADAM. All optimizers use the default $\beta_1, \beta_2, \epsilon \leftarrow 0.9, 0.999, 1e-8$. For PLUMAGE we reuse ADAM’s learning rate. In addition, we use a cosine decay schedule with a terminal value of 10% from the maximum learning rate and a linear warmup period for 10% of the total number of steps.

We run a learning rate grid search for the 130M and 350M models over 0.05, 0.01, 0.005, 0.0025, 0.001, 0.0075 to confirm the choice of the learning rate for PLUMAGE. We find that 0.001 consistently produces close to the best result, similar to the vanilla ADAM. To match the computational and memory budget between the methods, both low-rank gradient estimators use the same fixed projection update interval of $\tau = 200$ steps. We also match the rank for each model according to Zhao et al. [39]. Our approach, as shown in Table 3, consistently outperforms GALORE — without having to sweep over additional hyperparameters and without impacting the total train time. Moreover, training PLUMAGE was stable over multiple seeds, while in our experiments GALORE suffers from sharp fluctuations in the training loss, as well as training failures as the training loss diverged in some seeds.

Table 3: Token-level validation perplexity for pre-training with low-rank gradient estimators.

Method	130M	350M	1B
ADAM	25.95	19.02	14.3
GALORE	30.18	24.08	17.03
PLUMAGE _{S/MP}	28.73	21.81	16.29
Rank/Hidden	256/768	256/1024	512/2048
Tokens Seen	2.6B	7.9B	26.2B
Optimizer Steps	20K	60K	100K
Warmup Steps	2K	6K	10K

5 Discussion

Summary. In this work, we present PLUMAGE, a method to improve GALORE with similar computational and memory costs. Our method samples projections without replacement and yields a k -sparse and unbiased minimum variance estimator of the gradient. Our approach improves the accumulated projected statistics that are updated periodically during training. We demonstrate that our method can be used as a drop-in replacement for the full training procedure (without needing to re-tune the learning rate). During fine-tuning, we obtain similar accuracy as with standard (full-rank) training. During pre-training, we significantly decrease the degradation of GALORE compared to full-rank training. Notably, PLUMAGE has the potential to improve storage and communication in a wider context. The following applications do not dramatically change the optimization process from our experimental setup, yet we leave their in-depth exploration to future work.

Activation memory compression. Similarly to Shamshoum et al. [28], applying strictly right-sided PLUMAGE projections directly to linear layers’ inputs during the forward phase can lead to low-rank storage of activation, gradient, and optimizer state. This is mathematically equivalent to Eq. (27), albeit gradient projection cost is added to each training forward pass instead of just once per optimizer step, and gradient SVD cannot be done with gradient accumulation without additional memory.

Low-Rank Gradient Accumulation Buffers. The gradient size impacts both memory and communication costs throughout training. Moreover, when training with mixed precision, gradients are typically kept at higher precision. Thus, when both strategies are used for LLM training, gradient buffers are often distributed across the collective devices’ memory at the cost of significant communication overhead [26, 40]. Similarly to [16, 24], low-rank gradients via PLUMAGE can be accumulated directly into low-rank buffers as long as the projection is fixed between weight updates. Moreover, similarly to Wang et al. [36], PLUMAGE offers the additional benefit of using a device-specific low-rank projection to recover an estimate of the global batch gradient in a data-parallel setting, trading off compute overhead with communication and memory costs while halving the size of the communication overhead of ATOMO (since only one-sided projection is used).

References

- [1] A. F. Aji and K. Heafield. Sparse communication for distributed gradient descent. In *Proceedings of the 2017 Conference on Empirical Methods in Natural Language Processing*. Association for

- Computational Linguistics, 2017. doi: 10.18653/v1/d17-1045. URL <http://dx.doi.org/10.18653/v1/D17-1045>.
- [2] G. Alain, A. Lamb, C. Sankar, A. Courville, and Y. Bengio. Variance reduction in sgd by distributed importance sampling, 2015.
 - [3] R. Banner, I. Hubara, E. Hoffer, and D. Soudry. Scalable methods for 8-bit training of neural networks, 2018.
 - [4] Y. Blumenfeld, I. Hubara, and D. Soudry. Towards cheaper inference in deep networks with lower bit-width accumulators, 2024.
 - [5] X. Chen, C. Liang, D. Huang, E. Real, K. Wang, Y. Liu, H. Pham, X. Dong, T. Luong, C.-J. Hsieh, Y. Lu, and Q. V. Le. Symbolic discovery of optimization algorithms, 2023.
 - [6] B. Chmiel, L. Ben-Uri, M. Shkolnik, E. Hoffer, R. Banner, and D. Soudry. Neural gradients are near-lognormal: improved quantized and sparse training, 2020.
 - [7] B. Chmiel, I. Hubara, R. Banner, and D. Soudry. Minimum variance unbiased n:m sparsity for the neural gradients, 2022.
 - [8] M. Courbariaux, I. Hubara, D. Soudry, R. El-Yaniv, and Y. Bengio. Binarized neural networks: Training deep neural networks with weights and activations constrained to +1 or -1, 2016.
 - [9] T. Dettmers, M. Lewis, S. Shleifer, and L. Zettlemoyer. 8-bit optimizers via block-wise quantization, 2021.
 - [10] T. Dettmers, A. Pagnoni, A. Holtzman, and L. Zettlemoyer. Qlora: Efficient finetuning of quantized llms, 2023. URL <https://arxiv.org/abs/2305.14314>.
 - [11] C. Eckart and G. Young. The approximation of one matrix by another of lower rank. *Psychometrika*, 1(3):211–218, 1936.
 - [12] K. Fabian. How to sample exactly k indices given the inclusion probabilities of all indices?, 2024. URL <https://mathoverflow.net/q/475554>. URL: <https://mathoverflow.net/q/475554> (version: 2024-07-23).
 - [13] A. I. for AI. C4: Colossal clean crawled corpus. Dataset available at <https://huggingface.co/datasets/allenai/c4>, 2020.
 - [14] A. Gholami, Z. Yao, S. Kim, C. Hooper, M. W. Mahoney, and K. Keutzer. Ai and memory wall. *IEEE Micro*, 44(3):33–39, May 2024. ISSN 1937-4143. doi: 10.1109/mm.2024.3373763. URL <http://dx.doi.org/10.1109/MM.2024.3373763>.
 - [15] V. Gupta, T. Koren, and Y. Singer. Shampoo: Preconditioned stochastic tensor optimization, 2018.
 - [16] Y. Hao, Y. Cao, and L. Mou. Flora: Low-rank adapters are secretly gradient compressors, 2024.
 - [17] E. J. Hu, Y. Shen, P. Wallis, Z. Allen-Zhu, Y. Li, S. Wang, L. Wang, and W. Chen. Lora: Low-rank adaptation of large language models, 2021. URL <https://arxiv.org/abs/2106.09685>.
 - [18] I. Hubara, B. Chmiel, M. Island, R. Banner, J. Naor, and D. Soudry. Accelerated sparse neural training: A provable and efficient method to find n:m transposable masks. In M. Ranzato, A. Beygelzimer, Y. Dauphin, P. Liang, and J. W. Vaughan, editors, *Advances in Neural Information Processing Systems*, volume 34, pages 21099–21111. Curran Associates, Inc., 2021. URL https://proceedings.neurips.cc/paper_files/paper/2021/file/b0490b85e92b64dbb5db76bf8fca6a82-Paper.pdf.
 - [19] S. ichi Amari, R. Karakida, and M. Oizumi. Fisher information and natural gradient learning of random deep networks, 2018. URL <https://arxiv.org/abs/1808.07172>.
 - [20] D. P. Kingma and J. Ba. Adam: A method for stochastic optimization, 2017. URL <https://arxiv.org/abs/1412.6980>.

- [21] K. Liang, B. Liu, L. Chen, and qiang liu. Memory-efficient LLM training with online subspace descent. In *The Thirty-eighth Annual Conference on Neural Information Processing Systems*. NeurIPS, 2024. URL <https://openreview.net/forum?id=P8rTCT6g45>.
- [22] X. Liao, S. Li, Y. Xu, Z. Li, Y. Liu, and Y. He. Galore+: Boosting low-rank adaptation for llms with cross-head projection, 2024.
- [23] Y. Liu, M. Ott, N. Goyal, J. Du, M. Joshi, D. Chen, O. Levy, M. Lewis, L. Zettlemoyer, and V. Stoyanov. Roberta: A robustly optimized bert pretraining approach, 2019. URL <https://arxiv.org/abs/1907.11692>.
- [24] A. Muhamed, O. Li, D. P. Woodruff, M. Diab, and V. Smith. Grass: Compute efficient low-memory llm training with structured sparse gradients. *CoRR*, abs/2406.17660, 2024. URL <https://doi.org/10.48550/arXiv.2406.17660>.
- [25] C. Raffel, N. Shazeer, A. Roberts, K. Lee, S. Narang, M. Matena, Y. Zhou, W. Li, and P. J. Liu. Exploring the limits of transfer learning with a unified text-to-text transformer, 2019.
- [26] S. Rajbhandari, J. Rasley, O. Ruwase, and Y. He. Zero: Memory optimizations toward training trillion parameter models. In *SC20: International Conference for High Performance Computing, Networking, Storage and Analysis*, page 1–16. IEEE, Nov. 2020. doi: 10.1109/sc41405.2020.00024. URL <http://dx.doi.org/10.1109/SC41405.2020.00024>.
- [27] D. E. Rumelhart, G. E. Hinton, and R. J. Williams. Learning representations by back-propagating errors. *Nature*, 323(6088):533–536, 1986.
- [28] Y. Shamsoum, N. Hodos, Y. Sieradzki, and A. Schuster. Compact: Compressed activations for memory-efficient llm training, 2024. URL <https://arxiv.org/abs/2410.15352>.
- [29] N. Shazeer. Glu variants improve transformer, 2020.
- [30] N. Shazeer and M. Stern. Adafactor: Adaptive learning rates with sublinear memory cost, 2018.
- [31] M. Shoenberger, M. Patwary, R. Puri, P. LeGresley, J. Casper, and B. Catanzaro. Megatron-lm: Training multi-billion parameter language models using model parallelism, 2019.
- [32] H. Touvron, L. Martin, K. Stone, P. Albert, A. Almahairi, Y. Babaei, N. Bashlykov, S. Batra, P. Bhargava, S. Bhosale, D. Bikel, L. Blecher, C. C. Ferrer, M. Chen, G. Cucurull, D. Esiobu, J. Fernandes, J. Fu, W. Fu, B. Fuller, C. Gao, V. Goswami, N. Goyal, A. Hartshorn, S. Hosseini, R. Hou, H. Inan, M. Kardas, V. Kerkez, M. Khabsa, I. Kloumann, A. Korenev, P. S. Koura, M.-A. Lachaux, T. Lavril, J. Lee, D. Liskovich, Y. Lu, Y. Mao, X. Martinet, T. Mihaylov, P. Mishra, I. Molybog, Y. Nie, A. Poulton, J. Reizenstein, R. Rungta, K. Saladi, A. Schelten, R. Silva, E. M. Smith, R. Subramanian, X. E. Tan, B. Tang, R. Taylor, A. Williams, J. X. Kuan, P. Xu, Z. Yan, I. Zarov, Y. Zhang, A. Fan, M. Kambadur, S. Narang, A. Rodriguez, R. Stojnic, S. Edunov, and T. Scialom. Llama 2: Open foundation and fine-tuned chat models, 2023. URL <https://arxiv.org/abs/2307.09288>.
- [33] T. Vogels, S. P. Karimireddy, and M. Jaggi. Powersgd: Practical low-rank gradient compression for distributed optimization, 2020. URL <https://arxiv.org/abs/1905.13727>.
- [34] N. Vyas, D. Morwani, R. Zhao, M. Kwun, I. Shapira, D. Brandfonbrener, L. Janson, and S. Kakade. Soap: Improving and stabi lizing shampoo using adam, 2024.
- [35] A. Wang, A. Singh, J. Michael, F. Hill, O. Levy, and S. R. Bowman. Glue: A multi-task benchmark and analysis platform for natural language understanding, 2019. URL <https://arxiv.org/abs/1804.07461>.
- [36] H. Wang, S. Sievert, Z. Charles, S. Liu, S. Wright, and D. Papailiopoulos. Atomo: Communication-efficient learning via atomic sparsification, 2018.
- [37] T. Wolf, L. Debut, V. Sanh, J. Chaumond, C. Delangue, A. Moi, P. Cistac, T. Rault, R. Louf, M. Funtowicz, J. Davison, S. Shleifer, P. von Platen, C. Ma, Y. Jernite, J. Plu, C. Xu, T. L. Scao, S. Gugger, M. Drame, Q. Lhoest, and A. M. Rush. Huggingface’s transformers: State-of-the-art natural language processing, 2019.

- [38] B. Zhang and R. Sennrich. Root mean square layer normalization, 2019.
- [39] J. Zhao, Z. Zhang, B. Chen, Z. Wang, A. Anandkumar, and Y. Tian. GaLore: Memory-efficient LLM training by gradient low-rank projection. In R. Salakhutdinov, Z. Kolter, K. Heller, A. Weller, N. Oliver, J. Scarlett, and F. Berkenkamp, editors, *Proceedings of the 41st International Conference on Machine Learning*, volume 235 of *Proceedings of Machine Learning Research*, pages 61121–61143. PMLR, 21–27 Jul 2024. URL <https://proceedings.mlr.press/v235/zhao24s.html>.
- [40] Y. Zhao, A. Gu, R. Varma, L. Luo, C.-C. Huang, M. Xu, L. Wright, H. Shojanazeri, M. Ott, S. Shleifer, A. Desmaison, C. Balioglu, P. Damania, B. Nguyen, G. Chauhan, Y. Hao, A. Mathews, and S. Li. Pytorch fsdp: Experiences on scaling fully sharded data parallel. *Proceedings of the VLDB Endowment*, 16(12):3848–3860, Aug. 2023. ISSN 2150-8097. doi: 10.14778/3611540.3611569. URL <http://dx.doi.org/10.14778/3611540.3611569>.
- [41] P. Zhu and A. Knyazev. Angles between subspaces and their tangents. *Journal of Numerical Mathematics*, 21(4), Jan. 2013. ISSN 1570-2820. doi: 10.1515/jnum-2013-0013. URL <http://dx.doi.org/10.1515/jnum-2013-0013>.

Technical Appendices and Supplementary Material

A Measuring projection fitness via principal angles and adaptive projection intervals

Since applying SVD to each gradient at every step is costly, similarly to GALORE, we amortize the cost of SVD over multiple optimization steps, reusing the projection from an old gradient and updating it within some interval. However, since projected state optimizers [39, 21] converge despite using uncorrected statistics with alternating projections, we hypothesize that the dominant directions are relatively stable at least in some layers. Zhao et al. [39] also suggested that some layers require less frequent updates than others and proposed a per-layer adaptive interval controller to reduce the computational overhead of SVD. Specifically, the controller computes the cosine similarity between the first singular vectors of two subsequent projections to determine if the interval can be extended based on a fixed threshold. We argue that the suggested metric can be sensitive and unreliable. For example, if the ordering of singular vectors changes while the subspace remains unchanged, the proposed metric will return 0. In addition, when the correlation between subsequent subspaces breaks, the metric cannot be used to shrink the interval to reflect uncertainty.

We devise an alternative approach based on the framework of principal angles [41]. Namely, we calculate the cosine of the principal angle between the spanning subspaces can be retrieved by computing the singular values of $\mathbf{P}_1^\top \mathbf{P}_2 \in \mathbb{R}^{r_1 \times r_2}$ as follows,

$$\boldsymbol{\sigma} \leftarrow \text{SVD}(\mathbf{P}_1^\top \mathbf{P}_2). \quad (30)$$

Finally, we take the mean cosine angle to represent the intersection between the two induced subspaces.

$$\rho = \text{Mean}(\boldsymbol{\sigma}) \quad (31)$$

This approach offers a principled and robust measure for the overlap between subsequent projections during training. This approach allows our controller to manage the period between projection updates reliably. One specific advantage is the ability to reduce the interval when the assumptions regarding subsequent overlap break during training. In practice, we define a simple hysteresis controller with 3 threshold hyperparameters, γ_{shrink} , γ_{expand} , γ_{reset} that can be set by observing how well the training loss with a low-rank gradient estimator follows the loss of a standard optimizer and the recoded values of the principle angles with some fixed interval. The adaptive controller is given in Algorithm 1. In practice, the overlap can be approximated well with only the top 64 singular vectors from the old sampled projection matrix and the top 64 singular vectors from the freshly computed singular vectors of the new gradient (without sampling) to reduce the computational overhead of SVD when extracting the mean cosine principal angles. In addition, we find that allowing the interval to grow unconstrained undermines the original purpose of accelerating training, as it leads to degradation in the loss convergence rate and terminal value. Thus, we set a $\tau_{\text{max}} = 5\%$ of the total steps while $\tau_{\text{min}} = \tau_{\text{initial}} = 200$. Finally, we set $\gamma_{\text{shrink}}, \gamma_{\text{expand}}, \gamma_{\text{reset}} \leftarrow 0.4, 0.6, 0.3$ by observing the statistics during training, as can be seen in Figs. 4 and 5. We report the results in Table 4. Using our conservative adaptive interval hyperparameters, the equal-weighted average interval length over all layers in the models grew from the initial interval of 200 steps to ~ 425 steps and ~ 1000 steps for the 1B and 350M models. We observed minor terminal loss improvements in 1B and 350M models, potentially due to improved moment estimation with longer intervals. Ultimately, this avenue requires significant manual tuning to produce real train time gains while avoiding degradation in loss. Thus, we leave further exploration of this topic for future study utilizing larger models where the SVD overhead dominates the computation time.

Table 4: Token-level validation perplexity for pre-training with low-rank gradient estimators.

Method	130M	350M	1B
ADAM	25.95	19.02	14.3
GALORE	30.18	24.08	17.03
PLUMAGE _{S/MP}	28.73	21.81	16.29
PLUMAGE _{S/MP/A}	29.26	21.79	16.24
Rank/Hidden	256/768	256/1024	512/2048
Tokens Seen	2.6B	7.9B	26.2B
Optimizer Steps	20K	60K	100K
Warmup Steps	2K	6K	10K

Algorithm 1 Adaptive projection interval

inputs: subsequent projections $\mathbf{P}_{t-1}, \mathbf{P}_t \in \mathbb{R}^{m \times r}$, interval configurations $\tau_{\min}, \tau_{\max}, \tau_{\text{initial}}$, and thresholds $\gamma_{\text{reset}} \leq \gamma_{\text{shrink}} < \gamma_{\text{expand}} \in [0, 1]$
initialize: $\tau_0 \leftarrow \tau_{\text{initial}}, t \leftarrow 0$
 $\rho_t \leftarrow \text{mean_cosine_principle_angle}(\mathbf{P}_{t-1}, \mathbf{P}_t)$ \triangleright Eqs. (30) and (31)
if $\rho_t < \gamma_{\text{reset}}$ **then**
 $\tau_t \leftarrow \tau_{\min}$
else if $\rho_t < \gamma_{\text{shrink}}$ **then**
 $\tau_t \leftarrow \max(\tau_{t-1}/2, \tau_{\min})$
else if $\rho_t > \gamma_{\text{expand}}$ **then**
 $\tau_t \leftarrow \min(2 \cdot \tau_{t-1}, \tau_{\max})$
else
 $\tau_t \leftarrow \tau_{t-1}$
end if
 $t \leftarrow t + 1$
return: τ_t

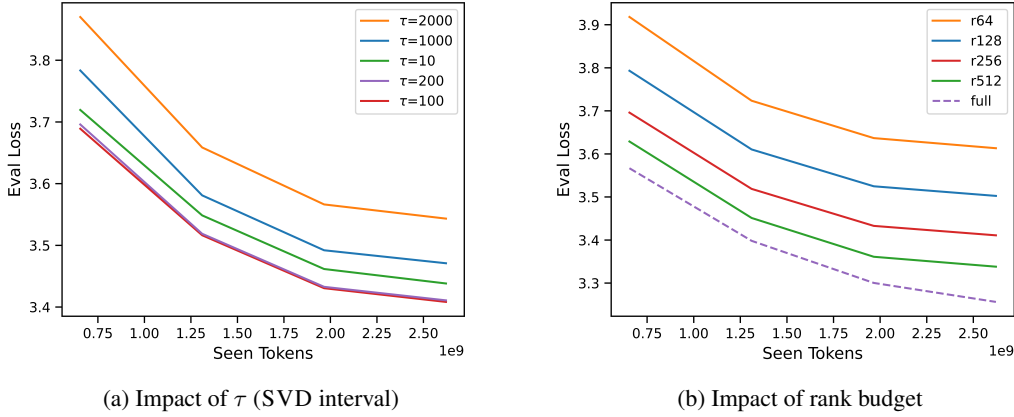


Figure 3: Ablation studies comparing validation loss Llama 130m on C4

B Additional qualitative experiments

B.1 Rank and interval ablation studies

We perform additional ablation experiments on the rank and SVD interval impact on the Llama 130M variant. The results are presented in Fig. 3. Similarly to Zhao et al. [39], we find that setting the gap interval too short or too wide leads to degradation in the optimization process. The short intervals potentially lead to poor first and second-moment estimates due to frequent projection updates. In addition, since $\mathbf{B} = \mathbf{P}_2^\top \mathbf{P}_1 \leq 1$ (see Section 3.3.3), the effective learning rate is also reduced. Finally, the choice of rank should be as large as one can fit onto the device memory, as can be seen in Fig. 3b.

B.2 Low-rank coverage quality

During training, we monitor the development of r^* and ρ for different layers. In Fig. 4, we show the progress of the metrics over time, and in (Figs. 5 and 6), we show the average values per-layer throughout the entire training. By tracking r^* in proportion to the total rank. We find that some layers, such as the attention projection layers, are more suitable for rank reduction. In contrast, the attention MLP down-projection layer parameters are the least amenable. This invites further exploration of rank budget allocation between different layers. For instance, stacking the QKV linear layers into a single matrix allows us to share a single low-rank projection matrix without impacting convergence while reducing SVD computational overhead. Moreover, the memory savings can be translated to increasing the rank of the less amenable layers, such as the MLP down layer, to improve the convergence within the same memory budget. We leave this topic to be explored in future work.

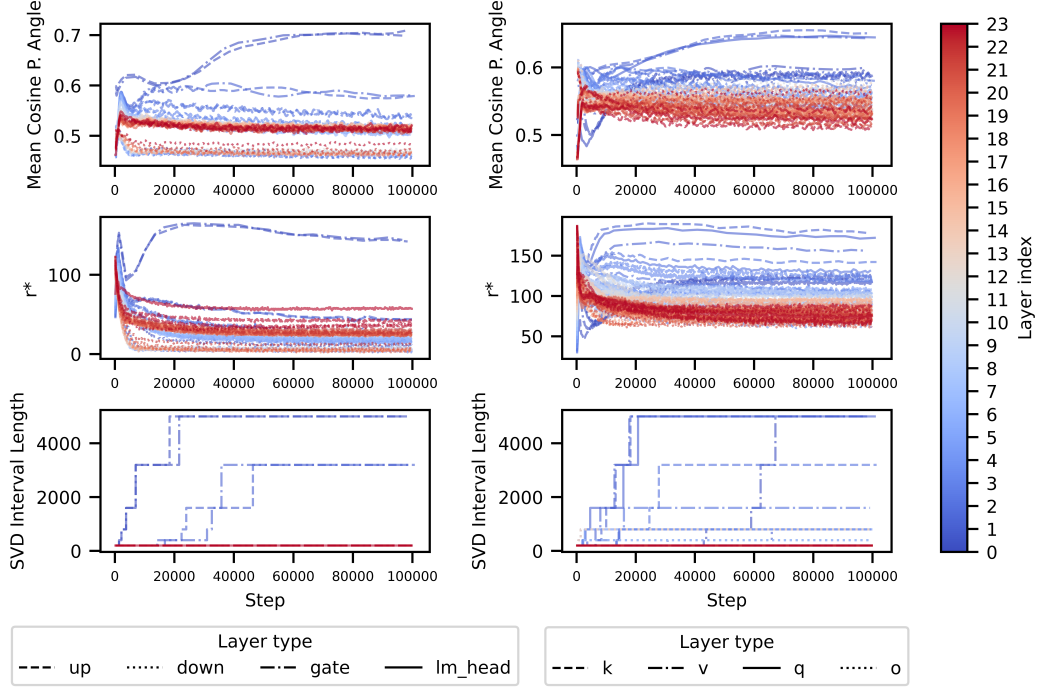


Figure 4: Tracking r^* (deterministic rank) and ρ (mean cosine principal angle) during pretraining of Llama 1B on C4 with PLUMAGE_{S/MP/A}

C Algorithms

C.1 Auxiliary algorithms

In this subsection, we present the algorithms for computing the PLUMAGE probabilities (Algorithm 2) and sampling from it exactly k indices (Algorithm 3) and constructing the projection matrices (Algorithm 4) as discussed in Sections 3 and 3.2. Note that all algorithms can be computed in $O(\min(m, n))$. This includes the reverse lookup via sorted search in Algorithm 3 that in case of naive implementation, requires $O(r \log(\min(m, n)))$; however since both arm pointers and target array are sorted, the implementation can continue to iterate over the target array as it locates the arm positions in sub-linear time.

Algorithm 2 COMPUTE_SAMPLING_PROBABILITIES(σ, k, ε)

- 1: **Inputs:** $\sigma \in \mathbb{R}^n$ (singular values, descending order), target rank k , numerical tolerance ε
 - 2: **Output:** deterministic rank r^* , inclusion probabilities $\mathbf{p} \in \mathbb{R}^d$
 - 3: $\mathbf{t} \leftarrow \text{reverseCumSum}(\sigma)$ $\triangleright t_i = \sum_{j=i}^d \sigma_j$
 - 4: $\mathbf{t} \leftarrow \max(\mathbf{t}, \varepsilon)$ \triangleright clip to avoid division by 0
 - 5: $\mathbf{i} \leftarrow (0, 1, \dots, n-1)$ \triangleright rank indices
 - 6: $\mathbf{s} \leftarrow k - \mathbf{i}$ \triangleright scaling factors $(k - r_t)$
 - 7: $\mathbf{q} \leftarrow (\mathbf{s} \odot \sigma) \oslash \mathbf{t}$ \triangleright test scores $q_i = \frac{(k-i)\sigma_i}{\sum_{j>i} \sigma_j}$
 - 8: $c \leftarrow |\{i \mid q_i < 1\}|$ \triangleright count how many ranks pass the test
 - 9: $r^* \leftarrow n - c$ \triangleright minimal rank that always enters ($r^* = d - c$)
 - 10: $\mathbf{p}_{0:r^*-1} \leftarrow 1$ \triangleright deterministic inclusion for top r^* modes
 - 11: $\mathbf{p}_{r^*:n-1} \leftarrow \frac{(k - r^*) \sigma_{r^*:n-1}}{t_{r^*}}$ \triangleright stochastic inclusion for remaining modes
 - 12: **return:** r^*, \mathbf{p}
-

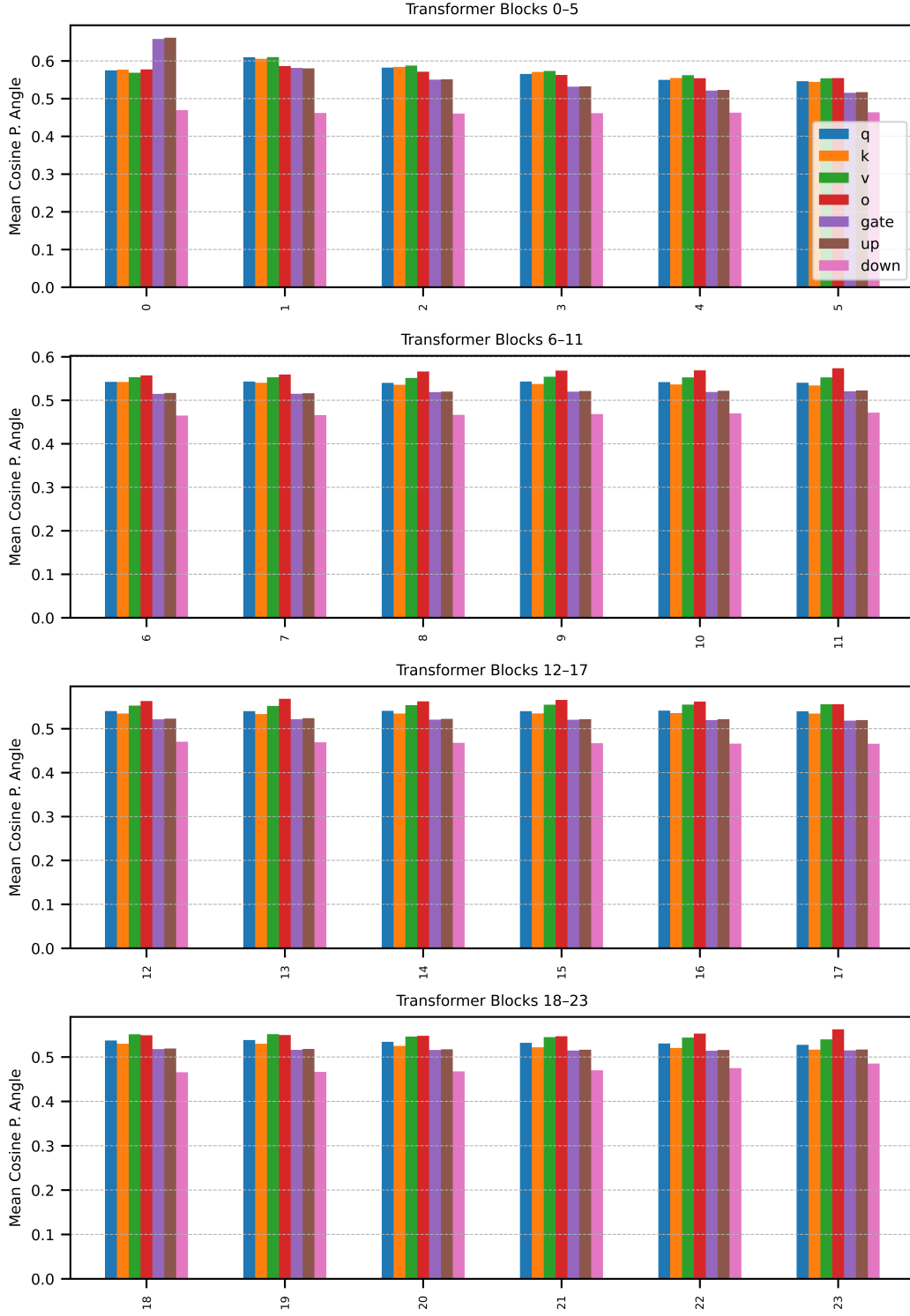


Figure 5: Mean ρ observed during Llama2-1B pretraining on C4 with rank=512

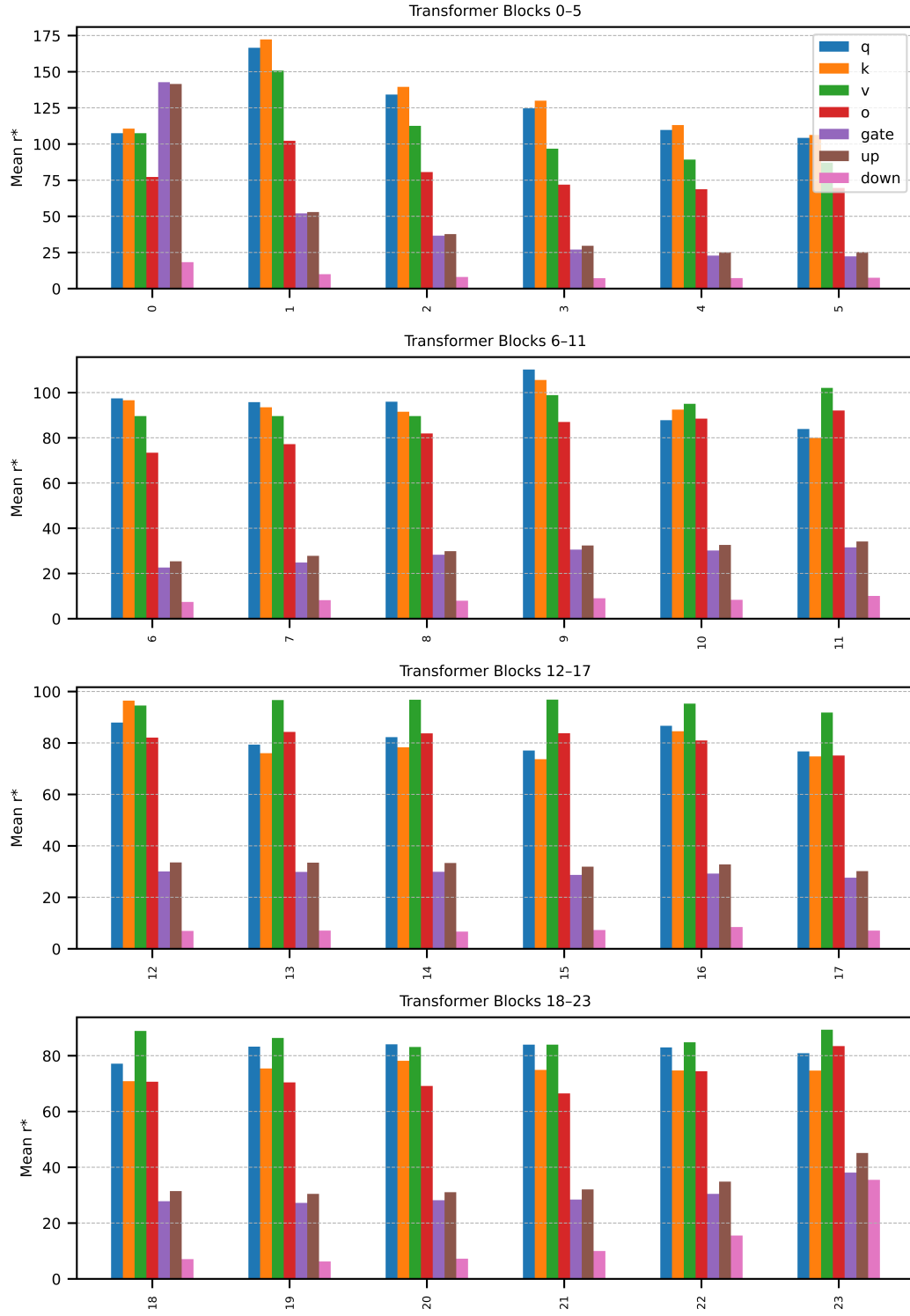


Figure 6: Mean r^* observed during LLama2-1B pretraining on C4 with rank=512

Algorithm 3 SAMPLE_INDICES(\mathbf{p}, k)

```
1: Inputs: inclusion probabilities  $\mathbf{p} \in \mathbb{R}^n$ , target sample size  $k$ 
2: Output: index set  $\mathcal{I} \subseteq \{0, \dots, n-1\}$ ,  $|\mathcal{I}| = k$ 
3:  $\tau \leftarrow \text{randPerm}(n)$  ▷ shuffle the indices
4:  $\mathbf{p}^{\text{sh}} \leftarrow \mathbf{p}[\tau]$  ▷ permute the probabilities
5:  $\mathbf{c} \leftarrow \text{cumSum}(\mathbf{p}^{\text{sh}})$  ▷  $c_i = \sum_{j=0}^i p_j^{\text{sh}}$ 
6:  $\delta \leftarrow \frac{\sum_{i=1}^n p_i^{\text{sh}}}{k}$  ▷ step size = total mass divided by  $k$ 
7:  $\beta \leftarrow \text{Uniform}(0, \delta)$  ▷ random offset
8:  $\mathbf{u} \leftarrow (0, \delta, \dots, (k-1)\delta) + \beta$  ▷  $k$  equally spaced pointers
9:  $\mathbf{j} \leftarrow \text{searchSorted}(\mathbf{c}, \mathbf{u})$  ▷ first index with  $c_j \geq \mathbf{u}$ 
10:  $\mathcal{I} \leftarrow \tau[\mathbf{j}]$  ▷ map back to original indices
11: return  $\mathcal{I}$ 
```

Algorithm 4 SAMPLE_PROJECTIONS($\mathbf{U}, \mathbf{p}, r$)

```
1: Inputs:  $\mathbf{U} \in \mathbb{R}^{m \times n}$  all singular vectors, column-stacked matrix (assuming  $m \leq n$ ),  $\mathbf{p} \in \mathbb{R}^n$ 
   sampling probabilities, target rank  $r$ 
2: Output: projections  $\mathbf{P} \in \mathbb{R}^{m \times r}$  and  $\mathbf{D} \in \mathbb{R}^{r \times r}$ 
3:  $\mathcal{I} \leftarrow \text{sample\_indices}(\mathbf{p}, r)$ 
4:  $\mathbf{P} \leftarrow \mathbf{U}[:, \mathcal{I}]$ 
5:  $\mathbf{D} \leftarrow \text{Diag}(\mathbf{p}[\mathcal{I}])$ 
6: return  $\mathbf{P}, \mathbf{D}$ 
```

C.2 PLUMAGE full algorithm

The main plumage algorithm is given in Algorithm 5. The computational cost is dominated by SVD ($O(d^3)$ assuming gradients are $\mathbb{R}^{d \times d}$ similarly to GALORE), which is hard to accelerate in hardware compared to matrix-matrix multiply (GEMM) since it requires sequential matrix-vector products. As mentioned in the previous section, the complexity of computing \mathbf{p} and sampling from it (Algorithm 4, Algorithm 2) is $O(d)$. We perform both algorithms after each SVD. Thus, the baseline PLUMAGE computational overhead is marginal compared to that of GALORE. In addition, State update methods (S/MP , Eqs. (28) and (29)) are dominated by GEMM operations with complexity $\mathbf{M}^l : O(d^2 r)$, \mathbf{B} and $\mathbf{V}^l : O(d^2 r)$. These operations are easy to accelerate on modern GPUs and are done once per SVD, amortizing their cost. Furthermore, in our experiments using A100/A6000 GPUs, we found that the total training time of our method, using unoptimized implementations, is unaffected by sampling and aligning of moments due to the dominance of SVD overhead. The memory footprint is similar to GaLoRE. It differs by the additional r sampling scale factors per layer. These can be offloaded to the host and prefetched before optimizer weight updates to maintain GaLoRE’s memory footprint. Finally, the adaptive SVD interval method ($S/MP/A$) requires computing the correlation matrix $\mathbf{P}_2^\top \mathbf{P}_1 \in \mathbb{R}^{r^2} : O(r^2 d)$ and SVD over the smaller matrix $O(r^3)$. This is done every time the SVD is computed on a new gradient, and the additional SVD step on the small $r \times r$ matrix can be done asynchronously to leverage underutilized compute time since it does not impact the weight update without concurrently storing the old and the fresh projection matrices.

D Experimental settings

Our pre-training experiment models are variants of Llama [32], as suggested by Zhao et al. [39]. These models utilize the same meta-architecture as Llama, except for RMS normalization layers [38] and SWIGLU activation functions [29]. The exact model configuration is given in Table 5. In all experiments, we used a single-node GPU server with 8xA100-40GB GPUs or 8xA100-80GB GPUs. The total compute time

Table 5: Model configurations.

Configuration	130M	350M	1B
Depth	12	24	24
Rank/Hidden	256/768	256/1024	512/2048
Intermediate	2048	2736	5461
Heads	12	16	32

Algorithm 5 Adam with PLUMAGE

inputs: linear layer weight $\mathbf{W} \in \mathbb{R}^{m \times n}$ with $m \leq n$, scalar loss function: $\mathcal{L} : \mathbb{R}^{m \times n} \rightarrow \mathbb{R}^1$, first and second moment decay rates β_1, β_2 , learning rate η , target rank r , number of optimization steps N , τ_0 number of steps between SVD, κ number of steps to resample projection.

initialize: $\mathbf{M}_0, \mathbf{V}_0 \in \mathbb{R}^{n \times r}, \mathbf{P}_0 \in \mathbb{R}^{m \times r} \leftarrow I, \leftarrow 0, t \leftarrow 0$.

repeat

$\mathbf{G}_t \leftarrow \nabla_{\mathbf{W}} \mathcal{L}(\mathbf{W}_t)$

if $t \bmod \tau_t = 0$ **or** $t \bmod \kappa = 0$ **then**

if $t \bmod \tau_t = 0$ **then**

$\mathbf{U}_t, \boldsymbol{\sigma}_t, \mathbf{V}_t \leftarrow \text{SVD}(\mathbf{G}_t)$

$r_t^*, \mathbf{p}_t \leftarrow \text{compute_sampling_probabilities}(\boldsymbol{\sigma}_t, r, \varepsilon = 1e-12)$

else

$\mathbf{U}_t, \boldsymbol{\sigma}_t, \mathbf{V}_t \leftarrow \mathbf{U}_{t-1}, \boldsymbol{\sigma}_{t-1}, \mathbf{V}_{t-1}$

end if

$\mathbf{P}_t, \mathbf{D}_t \leftarrow \text{sample_projection}(\mathbf{U}_t, \mathbf{p}_t, r)$

▷ Algorithm 4

$\mathbf{M}_t, \mathbf{V}_t \leftarrow \text{update_state}(\mathbf{M}_t, \mathbf{V}_t, \mathbf{P}_t, \mathbf{P}_{t-1})$

▷ Eqs. (28) and (29)

$\tau_{t+1} \leftarrow \text{update_interval}(\tau_t, \mathbf{P}_t, \mathbf{P}_{t-1})$

▷ Algorithm 1

else

$\mathbf{P}_t, \mathbf{D}_t \leftarrow \mathbf{P}_t, \mathbf{D}_{t-1}$

end if

$\mathbf{R}_t \leftarrow \mathbf{P}_t^\top \mathbf{G}_t$

$\mathbf{M}_t \leftarrow \beta_1 \cdot \mathbf{M}_{t-1} + (1 - \beta_1) \cdot \mathbf{R}_t$

$\mathbf{V}_t \leftarrow \beta_2 \cdot \mathbf{V}_{t-1} + (1 - \beta_2) \cdot \mathbf{R}_t^{\circ 2}$

$\mathbf{Z}_t \leftarrow \frac{\sqrt{1 - \beta_1^t}}{1 - \beta_1^t} \cdot \frac{\mathbf{M}_t}{\sqrt{\mathbf{V}_t} + \epsilon}$

$\mathbf{W}_t \leftarrow \mathbf{W}_t - \eta \cdot \mathbf{P}_t \mathbf{D}^{-1} \mathbf{Z}_t$

$t \leftarrow t + 1$

until $t = N$

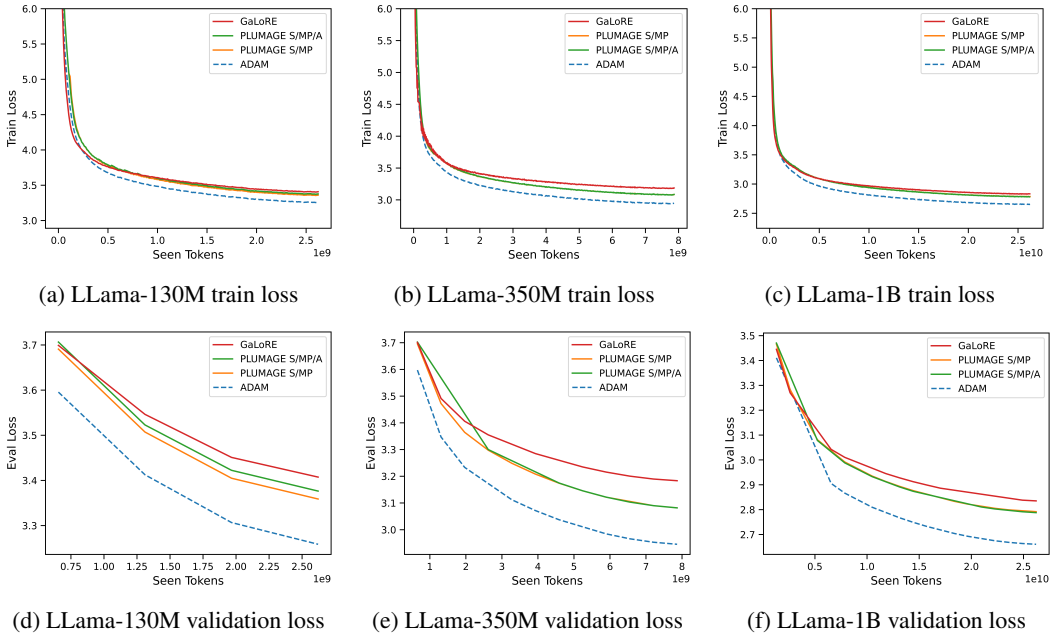


Figure 7: Pretraining loss plots of Llama on C4 datasets.

per experiment varied from ~ 9 GPU hours for the small 130M parameter model pre-training to ~ 620 GPU hours for the larger 1B model. We used a slightly modified version of Huggingface transformers [37] causal model training and GLUE finetuning code examples. We keep the model weights, gradients, and projections in the FP32 data type while using the BF16 mixed-precision support. In Fig. 7 we present the full validation and pretraining loss plots for pre-training experiments.